Giant enhancement of high-order rotational and rovibrational transitions in near-field spectroscopy in proximity to nanostructures

Asaf Farhi[1,2,*]

[1] *Department of Applied Physics, Yale University, New Haven, Connecticut, 06520, USA*
[2] *Department of Physics and Solid State Institute, Technion, Haifa 32000, Israel*

(Received 27 November 2022; revised 22 November 2023; accepted 1 March 2024; published 22 March 2024)

Vibrational-rotational and pure rotational transitions usually occur only via the electric dipole interaction channel and some molecules, such as homonuclear diatomics, do not have an electric dipole moment, rendering them transparent to infrared spectrum. We show that resonant nanostructures result in giant enhancement of high-order transitions in a relatively large volume, which implies an observable infrared signature for these molecules. The enhancement of these transitions may find applications in imaging, tissue ablation, resolving chiral molecules, and studies of molecules that are challenging to detect.

DOI: 10.1103/PhysRevApplied.21.034047

I. INTRODUCTION

Vibrations and rotations of molecules are quantized similarly to electronic states and the transitions between vibrational and rotational states are rotational, vibrational, or vibrational-rotational (rovibrational). Typically, the electronic degrees of freedom are the fastest, then the vibrational, and then the rotational. Thus, the frequencies of vibrational and rotational transitions are in the near infrared and microwave, respectively. While all of these transitions can be observed in gas phase, in solvent this is the case for electronic and vibrational transitions and there is usually no rotational spectrum since this motion is often restrained by the solvent [1]. Vibrational transitions are of high importance since light in the near-infrared window can penetrate into biological media longer distances [2]. Hence, their enhancement has potential use in biomedical applications [3–6], such as imaging and tissue ablation. In addition, rovibrational transitions have recently allowed the identification of water dimers, which are believed to affect Earth's radiation balance and climate, homogeneous condensation, and atmospheric chemistry [7].

Since the wavelength of a far field is typically much larger than the molecule size, usually only dipole rovibrational and pure rotational transitions with a rotational transition $\Delta J = \pm 1$ play a role in absorption spectroscopy and quantum computing [8]. However, diatomic homonuclear molecules such as H_2, N_2, and O_2 have no dipole rotational and vibrational transitions, and they are considered infrared inactive. Spherical top molecules, such as CH_4, SiH_4 have no rotational transitions in the rigid-rotor approximation and neglecting secondary effects no vibrational transitions of the symmetric modes [1,9,10]. In addition, due to the large difference between the wavelength and the molecule size, it is challenging to experimentally distinguish between chiral molecules, which are important in drug discovery, with a recent approach to improve this capability by enhancing the field chirality [11,12]. Interestingly, in the quasistatic regime the field is chiral [11,12] and there is an enhancement of the magnetic dipole, which may facilitate the ability to readily resolve chiral molecules. Moreover, photon detection, which is an enabling technology for quantum sensing and measurement-based quantum computing, is ineffective at triggering measurable phenomena at microwave frequencies since photons have 5 orders of magnitude lower energies compared with optical frequencies [13].

Enhancement and excitation of high-order electronic transitions have been widely discussed in the literature. Far-field excitation of high-order magnetic and electronic transitions, which are considered negligible, were theoretically analyzed long ago [14]. In the near field, it was shown that due to the shorter effective wavelength, the density of electromagnetic (EM) states significantly increases and there is enhancement of electric dipole and quadrupole transitions in proximity to dielectric and plasmonic materials [15–17]. Recently, a quantum electrodynamics (QED) theory to analyze the spontaneous emission of an atom in proximity to two-dimensional (2D) materials showed that they enable excitation of extremely high-order multipolar transitions, two-plasmon spontaneous emission, and singlet-triplet phosphorescence processes [18].

*asaf.farhi@yale.edu, asaf.farhi@gmail.com

Vibrational and rotational transitions of molecules have so far been analyzed mostly in the far field. Quadrupole infrared molecular transitions in the far field were studied theoretically long ago [19]. Later on, long pathlength spectroscopy enabled the observation of a weak quadrupole-allowed spectrum for N_2 and O_2 molecules in the far field [20] while the long interrogation times and high sensitivity of trapped-ion spectroscopy enabled the observation of quadrupole transitions in cold molecular N_2^+ ions [21]. Recently, enhancement of allowed vibrational transitions due to the increased density of EM states close to 2D structures has been observed experimentally [6]. More recently, enhancement of high-order multipolar pure rotational transitions close to a graphene ring with a circularly polarized incident light has been analyzed, focusing on electric field effects [22].

Here, we analyze the absorption of electromagnetic radiation via high-order rotational and rovibrational transitions, which are normally considered forbidden, by diatomic molecules in proximity to 2D materials, such as graphene and polar dielectric [23–29], see Fig. 1. These 2D materials have recently gained great attention as platforms to generate near-infrared and terahertz frequencies that are of importance in light-biomolecule interaction [32,33]. In our analysis, which is *semianalytical*, we consider the enhancement of light-molecule interaction with a plane-wave illumination due to *both* the shrinking of the electric field wavelength by the 2D structure (near-field effective wavelength compared with the far-field wavelength) and the increase of the density of EM states close to the structure, resulting in giant enhancement factors, with similar contributions. In addition, for a given confinement factor, 2D structures will enhance interactions at infrared frequencies in a larger volume compared to optical frequencies since the corresponding polarition decays slower spatially. We also relate our analysis to magnetic dipole transition enhancement and associated applications, such as resolving chiral molecules.

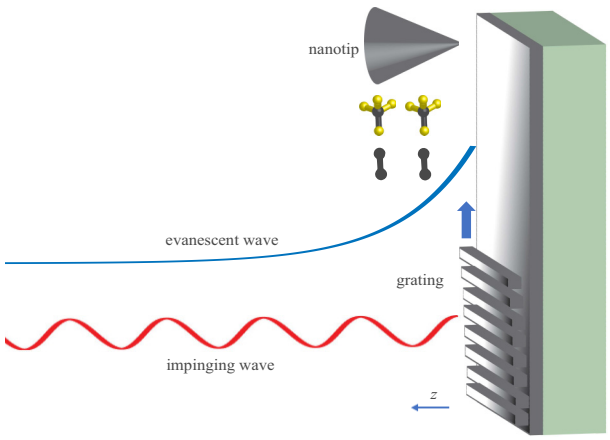

FIG. 1. A scheme of the setup: diatomic and spherical top molecules with no rotational-transition dipole moment in proximity to a 2D surface on a substrate. Far-field light is impinging on a periodic structure that excites a near-field mode of the 2D surface [23]. Since the evanescent field has high spatial frequency components, it enhances absorption via high-order rovibrational and rotational molecular transitions and enables absorption by molecules that otherwise have no rotational spectrum. The aborption spectrum can be measured by a near-field scanning optical microscopy tip, which couples the scattered field to the far field [30] or by the emission of the molecules after absorption. Alternatively, one could use a near-field scanning optical microscope in nanoscale Fourier-transform infrared spectroscopy [31].

In Sec. II we analyze quadrupole rovibrational and rotational absorption rates for homonuclear diatomic molecules in proximity to 2D structures. In Sec. III we calculate the absorption enhancement and integrated absorption for quadrupole transitions in N_2 molecules. Finally, Sec. IV includes a summary of our results and a discussion on potential applications.

II. QUADRUPOLE ROVIBRATIONAL AND ROTATIONAL TRANSITION RATES OF DIATOMIC MOLECULES IN PROXIMITY TO 2D STRUCTURES

We now investigate quadrupole selection rules and transition rates of homonuclear diatomic molecules having a $^1\Sigma_g^+$ ground electronic state, i.e., a singlet state and zero angular momentum (most stable molecules have $^1\Sigma_g^+$ ground states, notable exceptions being O_2 and NO [9]). In the adiabatic approximation, in which there is negligible coupling between the electronic, vibrational, and rotational degrees of freedom, the wave function of a molecule becomes $\psi \approxeq \psi_{\mathrm{el}}\psi_{\mathrm{N}}$, where ψ_{el} and ψ_{N} are the electronic and nuclear wave functions, respectively. ψ_{N} for a homonuclear diatomic molecule can be approximated as [9]

$$\psi_{\mathrm{N}} \approxeq \frac{S_v(\tilde{r})}{f} R Y_J^M(\theta_{\mathrm{N}}, \phi_{\mathrm{N}}),$$

$$S_v(\tilde{r}) = \left(\frac{\alpha}{\pi}\right)^{1/4} \frac{1}{(2^v v!)^{1/2}} H_v\left(\alpha^{1/2}\tilde{r}\right) e^{-\alpha\tilde{r}^2/2},$$

where $S_v(\tilde{r})$ and Y_J^M are harmonic oscillator and spherical harmonic wave functions, respectively, R is the internuclear distance, H_v is a Hermite polynomial, $\tilde{r} = R - R_e$, $\alpha = 4\pi^2 \nu_e \mu/h$, $\mu = m_a m_b/(m_a + m_b)$, $\nu_e = 1/2\pi\,(k_e/\mu)^{1/2} = 1/2\pi\left(U''(R_e)/\mu\right)^{1/2}$, and R_e is the equilibrium distance [9]. Note that J is the rotational quantum number, M is its z-axis projection that is measured with respect to laboratory frame, and there is only a relation between the quantum numbers J, M unlike the situation in the electronic states in hydrogen atoms, where

the range of the electronic quantum number l depends on n. The negligible coupling between the vibrational and rotational degrees of freedom is valid when $E_v \gg E_J$ or $h\nu_e \gg hBJ\,(J+1)$, where the rotational constant $B = h/4\pi I, I = \mu r_e^2$. While this usually holds, for small molecules such as H_2 at large rotational numbers, one needs to account for the rovibrational coupling [19].

We now proceed to the Fermi golden rule calculation of the absorption rate. The Hamiltonian of interest is given by [34]

$$H = H_0 + H_{\text{int}}, \quad H_0 = \sum_i \frac{P_i^2}{2m_i} + V(r),$$
$$H_{\text{int}} = -\frac{q}{m}\mathbf{P}\cdot\mathbf{A} - \frac{q}{m}\mathbf{S}\cdot\mathbf{B} + \frac{q^2}{2m}[\mathbf{A}]^2,$$

where $\mathbf{A}$ is the magnetic vector potential satisfying $\mathbf{B} = \nabla\times\mathbf{A}, \mathbf{E} = -\nabla\phi - (\partial\mathbf{A}/\partial t)$, $\mathbf{S}$ is the spin vector, and H_0 is the entire Hamiltonian without an electric field, where the motion of the center of mass is separated from the relative motion of the particles. By expanding the first term in H_{int} for an evanescent electric field $\mathbf{E} \propto E_1 e^{-i\omega t + ik_y y - k_z z}$, where the z axis is perpendicular to the 2D structure, we obtain

$$\begin{aligned}\mathbf{P}\cdot\mathbf{A} &= \frac{E_1}{i\omega}\left(-iP_z + P_{\mathbf{k}_\parallel}\right)\cdot e^{-i\omega t + ik_y y - k_z z}\left(-i\mathbf{e_z} + \mathbf{e}_{\mathbf{k}_\parallel}\right)\\ &\approx \frac{E_1}{i\omega}\left(-iP_z + P_y\right)\cdot e^{-i\omega t}\left(1 + ik_y y - k_z z\right)\\ &\quad\times\left(-i\mathbf{e_z} + \mathbf{e}_{\mathbf{k}_\parallel}\right),\end{aligned}$$

where $k_z \gg k = 2\pi/\lambda = k_z^2 - |\mathbf{k}_\parallel|^2$, $\mathbf{k}_\parallel = (k_x, k_y)$ is a 2D vector in a direction parallel to the slab, and Coulomb gauge has been used. We now show that in the quadrupole operator one can replace P_i by x_i. To that end, we express the quadrupole term $P_z Y$ as follows:

$$\begin{aligned}P_z Y &= \frac{1}{2}\left(P_z Y - ZP_y\right) + \frac{1}{2}\left(P_z Y + ZP_y\right)\\ &= \frac{1}{2}L_x + \frac{1}{2}\left(P_z Y + ZP_y\right).\end{aligned}$$

L_x can be grouped with $\mathbf{S}\cdot\mathbf{B}$ and the second term becomes [34]

$$\begin{aligned}P_z Y + ZP_y &= \frac{m}{i\hbar}\left\{[Z, H_0]\,Y + Z\,[Y, H_0]\right\}\\ &= \frac{m}{i\hbar}\left(ZYH_0 - H_0 ZY\right).\end{aligned}$$

We analyze a transition between two eigenstates of H_0 ψ_f, ψ_i via this quadrupole operator

$$\begin{aligned}\left\langle\psi_f\left|P_z Y + ZP_y\right|\psi_i\right\rangle &\propto \left\langle\psi_f\left|\frac{k_y}{i\omega}\frac{q}{\hbar}E_z\left(ZYH_0 - H_0 ZY\right)\right|\psi_i\right\rangle\\ &= -ik_y q E_z\left\langle\psi_f\left|ZY\right|\psi_i\right\rangle,\end{aligned}$$

where H_0 operated on the eigenstates in the last transition and we assumed $|\omega - \omega_{if}| \ll \omega_{if}$ [34]. Hence, we observe that all in all $P_z Y \to ZY$ and therefore $P_z \to Z$. The quadrupole term can thus be written as

$$\left\langle\psi_f\left|\mathbf{P}\cdot\mathbf{A}\right|\psi_i\right\rangle_{\text{quad}} \propto \frac{\partial E_j}{\partial x_i}\left\langle\psi_f\left|x_j x_i\right|\psi_i\right\rangle.$$

Now we write the quadrupole transition rate between nuclear states $N \to N'$ using Fermi's golden rule

$$\begin{aligned}\left(\Gamma_{\text{N}'\to\text{N}}\right)_{\text{quad}} = \frac{\pi}{2\hbar}\rho\Bigg|\sum_i\sum_j \frac{\partial E_j}{\partial x_i}(0)\\ \times\left\langle\psi_{\text{N}}\right|\left(\int\psi_{\text{el}}^* Q_{ij}\,\psi_{\text{el}}dr'\right)\left|\psi_{\text{N}'}\right\rangle\Bigg|^2,\end{aligned}$$

where

$$Q_{zz}(r) = -\frac{1}{2}\int\left(3z'^2 - r'^2\right)\zeta_r^{\text{mol}}\left(r, r'\right)dV' + \frac{Z_a r^2}{2},$$
$$Q_{xx}(r) = Q_{yy}(r) = -\frac{1}{2}\int\left(3x'^2 - r'^2\right)\zeta_r^{\text{mol}}\left(r, r'\right)dV',$$

and r', r denote the electronic and nuclear degrees of freedom, respectively, ρ is the density of EM states at the transition frequency, Z_a is the atomic number of the nuclei, and $\zeta_r^{\text{mol}}\left(r, r'\right)$ is the electron charge density. Upon integration over the electronic degrees of freedom, the quadrupole operator will depend on the nuclear configuration, such that

$$\Gamma_{\text{N}'\to\text{N}} = \frac{\pi}{2\hbar}\rho\left|\sum_{i,j,l}\frac{\partial E_j}{\partial x_i}(0)\left\langle\psi_{\text{N}}\right|Q_{ll}(r)\,D_{li}D_{lj}\left|\psi_{\text{N}'}\right\rangle\right|^2,$$

where $D_{\text{lab}\to\text{mol}} \equiv$

$$\begin{pmatrix}\cos\theta_{\text{N}}\cos\phi_{\text{N}} & \cos\theta_{\text{N}}\sin\phi_{\text{N}} & -\sin\theta_{\text{N}}\\ -\cos\theta_{\text{N}}\sin\phi_{\text{N}} & \cos\theta_{\text{N}}\cos\phi_{\text{N}} & -\sin\theta_{\text{N}}\\ \sin\theta_{\text{N}}\cos\phi_{\text{N}} & \sin\theta_{\text{N}}\sin\phi_{\text{N}} & \cos\theta_{\text{N}}\end{pmatrix}.$$

We then approximate $Q_{zz}(r)$ close to the equilibrium distance between the atoms R_e [35]

$$Q_{zz}(r) \approx Q_{zz}(R_e) + \left(\frac{dQ_{zz}(r)}{dr}\right)_{R_e}\tilde{r} + \left(\frac{d^2 Q_{zz}(r)}{dr^2}\right)_{R_e}\frac{\tilde{r}^2}{2},$$

where $\tilde{r} \equiv r - R_e$. We analyze the radial part of $\Gamma_{N' \to N}$

$$\int \left(Q_{zz}(R_e) + \left(\frac{dQ_{zz}(r)}{dr} \right)_{R_e} \tilde{r} + \left(\frac{d^2 Q_{zz}(r)}{dr^2} \right)_{R_e} \frac{\tilde{r}^2}{2} \right) \times S_v(\tilde{r}) S_{v'}(\tilde{r}) \, d\tilde{r},$$

and see that the first, second, and third terms correspond to the *vibrational* selection rules $v' = v, v' = v \pm 1$, and $v' = v \pm 2, v' = v$, respectively, and $\left| \langle v' | \tilde{r} | v \rangle \right|^2 = (v+1)/2\alpha$ [9]. Q_{zz} and its derivatives have been calculated for several diatomic molecules using quantum chemistry calculations in Ref. [35]. By observing the effect of the D matrix on the rotational states, one can see that for the quadrupole transition $\Delta J = 0, \pm 2$. To account for the angular part of the inner product, we incorporate the Clebsh-Gordan coefficients $C(J2J'; 00)^2$ [36], which can be used due to the similarity of the evanescent wave to a plane wave, and lead to the following factors:

$$\begin{cases} 3(J+1)(J+2)/2(2J+1)(2J+3) & J' = J+2 \\ J(J+1)/(2J-1)(2J+3) & J' = J \\ 3J(J-1)/2(2J-1)(2J+3) & J' = J-2 \end{cases}.$$

From the dependence of the square of the inner product on $\partial E_j / \partial x_i$ we deduce the following general scaling:

$$\left| \langle \psi_f | \mathbf{P} \cdot \mathbf{A} | \psi_i \rangle_n \right|^2 \propto \eta^{2(n-1)} e^{-2k_z z_0},$$

where n is the order of the interaction ($n = 2$ for quadrupole transitions), z_0 is the molecule location, and $\eta = 2\pi/(\lambda k_z)$ is the confinement factor. For a lossless graphene [18,37] we obtain ρ using a semiclassical calculation (see Appendix for details)

$$\rho = -\frac{2\omega}{\pi} \mathrm{Im}\left[G_{\mu\mu}(\mathbf{x}, \mathbf{x}, \omega) \right] = \frac{\omega}{(2\pi^2)} \left(k\eta^3 \frac{1}{(\epsilon_r + 1)} e^{-2k\eta z_0} \right),$$

where ϵ_r is the permittivity of the substrate. In free space $\rho \propto \omega^3$ [38] and, therefore, light-matter interactions are expected to be stronger at high frequencies (for the same inner product).

At room temperature the molecules are mainly in the ground vibrational state and we express the density of molecules at a rotational state J as

$$n = n_0 g_{nT} \frac{(2J+1) e^{-BhJ(J+1)/k_B T}}{\mathcal{Z}},$$

where n_0 is the total density of the molecules, g_{nT} is the nuclear spin degeneracy, and the partition function reads [9]

$$\mathcal{Z} = \sum_{J=0}^{\infty} g_{jn} (2J+1) e^{-BhJ(J+1)/k_B T}.$$

Thus, overall the absorption for rovibrational and pure rotational transitions scales as

$$\Gamma_{N' \to N} \propto \omega k \eta^3 k^{2(n-1)} \eta^{2(n-1)} e^{-4k_z z_0}.$$

This is similar to the scaling of spontaneous emission in high-order electronic transitions involving a change in l calculated using QED, $\Gamma_{l' \to l} \propto \eta^3 \eta^{2(n-1)} e^{-2k_z z_0}$ [18], except for the additional factor $e^{-2k_z z_0}$, that originates from the electric field $\mathbf{E}$ in our absorption calculation. However, rovibrational and especially rotational transitions have very long wavelengths and therefore the enhancement factors can be significantly larger. In addition, the field that impinges on the grating or tip will scatter and experience near-field enhancement by the 2D structure as we explain below [39,40]. The same scaling found for the quadrupole transitions is also expected to occur for magnetic dipole transitions, with the potential application of resolving chiral molecules [11,12,41]

To calculate g_{jn} we recall from the Pauli exclusion principle that particles with integer (half integer) nuclear spin have symmetric (antisymmetric) total wave functions, which can be decomposed as follows:

$$\psi_{\mathrm{tot}} \approx \psi_{\mathrm{tran}} \psi_{\mathrm{vib}} \psi_{\mathrm{el}} \psi_{\mathrm{rot}} \psi_{\mathrm{nuc\ spin}},$$

where ψ_{tran} and ψ_{vib} are not affected by $r \to -r$ for a diatomic homonuclear molecule. ψ_{el} is symmetric for molecules in ground state ${}^1\Sigma_g^+$ such as N_2. ψ_{rot} is symmetric and antisymmetric for even and odd J, respectively. The degeneracy of $\psi_{\mathrm{nuc\ spin}}$ reads

$$\begin{aligned} &\text{symmetric } (2I+1)(I+1), \\ &\text{antisymmetric } (2I+1) I, \end{aligned}$$

where I is the nuclear spin quantum number. For example, N_2 has $I = 1$ and a nuclear spin degeneracy of 3 and 6 for the antisymmetric and symmetric wave functions, respectively. Therefore, since the nuclear of N is a boson (integer spin) and ψ_{tot} is symmetric, the even and odd J eigenfunctions have a degeneracy of 6 and 3, respectively.

We now multiply the density of molecules at a rotational state J by ρ and the square of the inner product to get the integrated absorption in the transition $v, J \to v', J'$:

$$A_0 = n_0 \frac{g_{jn}(2J+1) e^{-BhJ(J+1)/k_B T}}{\mathcal{Z}} \times \rho \sum_{M,M'} \left| \langle \psi_{\Sigma,v',J',M'} | H_{\mathrm{QE}} | \psi_{\Sigma,v,J,M} \rangle \right|^2.$$

where $H_{\mathrm{QE}} \propto \sum_{i,j} (\partial E_j/\partial x_i)(0) Q_{ij}$. It can be deduced from hB/k_BT that the population is usually maximal for an intermediate value of J, which explains the intensity pattern in the rovibrational bands. Finally, another effect to consider is the field enhancement due to the near-field resonance of the nanostructure, which can increase the absorption by 4–6 orders of magnitude, depending on the material losses [39,40].

The energy of a rovibrational level is approximated as [9]

$$E \approx U(R_e) + h\nu_e \left(v + \frac{1}{2}\right) + hBJ(J+1).$$

Thus, for the quadrupole transitions $\Delta J = \pm 2$ we get

$$\Delta E_{J\to J-2} = -hB(4J-2), \quad \Delta E_{J\to J+2} = hB(4J+6),$$

and the energy shifts become larger as the initial J increases. Importantly, even if the pure rotational transitions with a small initial J and $\Delta E \sim 4hB$, have a large wavelength compared to the polariton spectrum of the 2D structure, the transitions with a high initial J can be in the spectrum. The rotationless $v = 0 \to 1$ energy shift can be readily approximated as $\Delta E_{v=0\to 1} = h\nu_e$.

III. QUADRUPOLE ABSORPTION RATES FOR N_2 MOLECULES

For concreteness, we consider an ensemble of N_2 molecules in proximity to a 2D structure. In Fig. 2 we plot the enhancement factors of the quadrupole rovibrational and pure rotational transitions compared with free space as functions of the distance from the 2D structure, where we assumed field enhancement of four orders of magnitude. While the rovibrational transition is enhanced by approximately 9 orders of magnitude a few nanometers away from the structure, the pure rotational transition is enhanced by approximately 22 orders of magnitude for the same near-field profile due to the η^5 in the overall scaling. To estimate the enhancement required for absorption on the order of the standard far-field dipole transition absorption, we recall the field expansion and express this enhancement as follows: $1/(kr)^2 \approx 1/(kl)^2 \approx (\lambda/l)^2$, where l is the wave-function extent, which is approximately the molecule size. Thus, we get that for quadrupole rovibrational and rotational transitions approximately 8 and 14 orders of magnitude of enhancement are required, respectively. Alternatively, for the same confinement factor a much larger volume will be covered for enhancing pure rotational transitions since the polariton wavelength is larger and it therefore decays more slowly spatially. Note that in practice the enhancement will be affected by the absorption in the nanostructure as well as the experimental technique. Note also that 2D structures with incident fields in the terahertz were realized experimentally and our calculations show that pure rotational quadrupole transitions of N_2 with initial $J \geq 2$ can be observed [28]. For approaches of detecting terahertz radiation in the near field and far field, see Refs. [42–44].

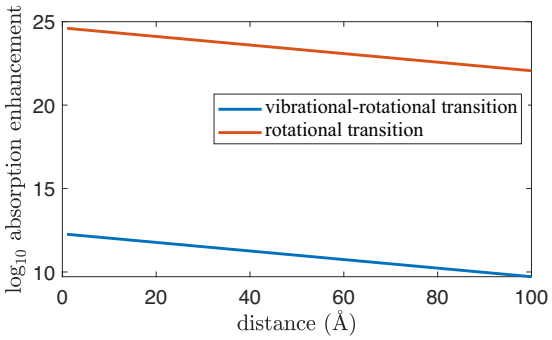

FIG. 2. Enhancement of the absorption via the vibrational-rotational $v = 0 \to 1, \Delta J = 2$ and pure rotational $J = 0 \to 2$ quadrupole transitions of an N_2 molecule in proximity to the 2D structure as functions of distance.

We then calculate the absorption due to $v = 0 \to 1$ rovibrational quadrupole transitions in N_2 molecules. where we have used $(dQ_{zz}(r)/dr)_{R_e} = 0.94\,(ea_0)$, $\tilde{\nu} = 2329\ (\mathrm{cm}^{-1})$ [35], and $\tilde{B} = 2.01\ (\mathrm{cm}^{-1})$. These transitions become dominant due to the proximity to the resonant structure, which results in an infrared signature for these molecules. In Fig. 3 we present the normalized integrated absorption as a function of the wave number for molecules situated 100 Å from the 2D surface and a polariton that has 100 times smaller effective wavelength compared to the incident λ. 2D structures with such λ values and even larger confinement factors were experimentally demonstrated [27,29]. It can be seen that the strong transitions are for intermediate values of J due to the population of these levels and the transitions for even J are stronger due to the higher nuclear-spin degeneracy, as expected. Clearly, the intensity of the $\Delta J = 0$ transition is rather high since it includes all the initial J states (neglecting the effect of centrifugal distortion, which results in very small splitting). It is worth noting that in the near field the spatial distribution of the electric field is independent of frequency for a given $\epsilon(\mathbf{r})$ [45]. However, transitions at these infrared frequencies that may be weak in the far field, can play a dominant role in proximity to nanostructures, which is important due the ability of radiation in the near infrared to penetrate more into biological media and excite vibrational transitions (e.g., $\Delta J = 0$ in Fig. 3).

IV. SUMMARY

In summary, we have analyzed the absorption of an electric field by molecules in the vicinity of a 2D structure via high-order rovibrational and rotational transitions.

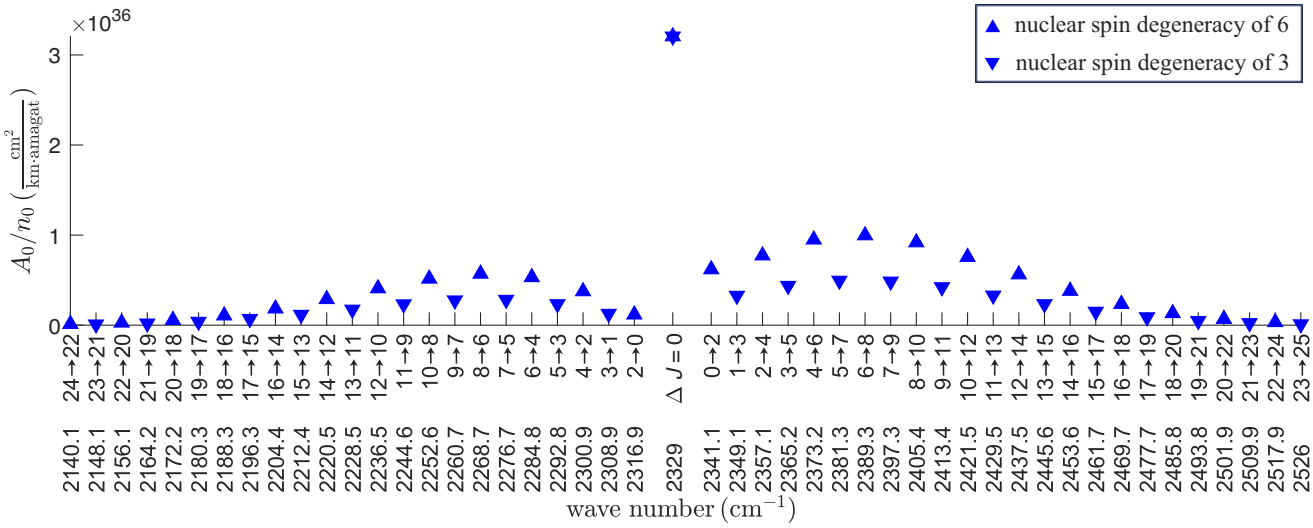

FIG. 3. Normalized integrated absorption A_0/n_0 for $v = 0 \to 1$ rovibrational quadrupole transitions as a function of the wave number for an N_2 molecule situated 100 Å from 2D graphene with $\eta = 100$. The central $v = 0 \to 1, \Delta J = 0$ Q-branch absorption frequency corresponds to $\lambda = 4.25$ μm and the rotational energy difference for $\Delta J = 2$, $4Bh$ corresponds to $\lambda = 1.25$ mm. An enhancement factor of approximately 10^9 is achieved compared with quadrupole transitions of molecule situated in free space.

We have shown that due to the presence of a 2D structure, which generates a short wavelength polarition and increases the density of EM states, molecules without an electric dipole moment, such as homonuclear diatomic, become infrared active. While there is enhancement of both rovibrational and rotational transitions, rotational transitions can be enhanced by many more orders of magnitude provided that the propagating field at the corresponding frequency can be coupled to short-wavelength surface modes of the 2D structure [28]. The enhancement of the absorption in high-order transitions may find applications in noninvasive tissue ablation [3–5] and resolving chiral molecules [11,12] and molecules that are challenging to detect. This analysis can be applied to dipole and higher-order rotational transitions, which are also expected to be observable in proximity to 2D structures. From similar arguments, enhancement of high-order rotational transitions associated with spontaneous emission and Forster resonance energy transfer (FRET) can be predicted [18,46–48].

ACKNOWLEDGMENTS

P. H. Vaccaro is greatly acknowledged for the continuous feedback, corrections, and pointing out additional applications. H. Suchowski, T. Schwartz, C. Fleischer, O. Cheshnovsky, I. Kaminer, and N. Rivera are acknowledged for the insightful comments. The anonymous reviewers are highly acknowledged for the comprehensive reviews, which improved the paper.

APPENDIX A: CALCULATING THE DENSITY OF ELECTROMAGNETIC STATES

We present a semiclassical calculation of the density of electromagentic states in the vicinity of a 2D graphene deposited on a substrate. Generally, the density of states can be written as [37,49]

$$\rho_\mu = -\frac{2\omega}{\pi}\mathrm{Im}(G_{\mu\mu}(\mathbf{x},\mathbf{x},\omega)).$$

For an evanescent wave we can write [18]

$$\rho_{k,z} = \frac{2\omega}{\pi}\mathrm{Im}\frac{i}{2}\frac{1}{(2\pi)^2}\int d\mathbf{q}c^2\frac{r_p q}{\omega_0^2}\left(\frac{k_\perp}{q},-\frac{q}{k_\perp}\right)e^{2ik_\perp z_0}.$$

Taking the quasistatic limit $k_\perp = iq$ we obtain

$$\rho_{k,z} = \frac{2\omega}{\pi}\mathrm{Im}\left(-\frac{1}{2}\frac{1}{(2\pi)^2}\int d\mathbf{q}c^2\frac{r_p q}{\omega_0^2}e^{-2qz_0}(1,-1)\right).$$

We substitute the Fresnel reflection coefficient for graphene $r_p = (\epsilon_r - 1)\,i - (\sigma q/\omega_0\epsilon_0)/(\epsilon_r + 1)\,i - (\sigma q/\omega_0\epsilon_0)$, where ϵ_r is the permittivity of the substrate on which the graphene is deposited [18] and σ is the electric conductivity, and get for each orientation

$$\rho = -\frac{\omega}{\pi}\frac{c^2}{(2\pi)^2}\mathrm{Im}\left(\int d\mathbf{q}\frac{(\epsilon_r - 1)\,i - \frac{\sigma q}{\omega_0\epsilon_0}}{(\epsilon_r + 1)\,i - \frac{\sigma q}{\omega_0\epsilon_0}}\frac{q}{\omega_0^2}e^{-2qz_0}\right).$$

Substituting complex σ

$$\begin{aligned}
\rho &= -\frac{\omega}{\pi}\frac{c^2}{(2\pi)^2}\mathrm{Im}\left(\int d\mathbf{q}\frac{(\epsilon_r-1)\,i-\frac{(\sigma_R+i\sigma_I)q}{\omega_0\epsilon_0}}{(\epsilon_r+1)\,i-\frac{(\sigma_R+i\sigma_I)q}{\omega_0\epsilon_0}}\frac{q}{\omega_0^2}e^{-2qz_0}\right)\\
&= -\frac{\omega}{\pi}\frac{c^2}{(2\pi)^2}\mathrm{Im}\left(\int d\mathbf{q}\frac{(\epsilon_r-1)\,i-\frac{\sigma_R q}{\omega_0\epsilon_0}-\frac{i\sigma_I q}{\omega_0\epsilon_0}}{(\epsilon_r+1)\,i-\frac{\sigma_R q}{\omega_0\epsilon_0}-\frac{i\sigma_I q}{\omega_0\epsilon_0}}\frac{q}{\omega_0^2}e^{-2qz_0}\right)\\
&= -\frac{\omega}{\pi}\frac{c^2}{(2\pi)^2}\mathrm{Im}\left(\int d\mathbf{q}\frac{-\frac{\sigma_R q}{\omega_0\epsilon_0}+i\left[(\epsilon_r-1)-\frac{\sigma_I q}{\omega_0\epsilon_0}\right]}{-\frac{\sigma_R q}{\omega_0\epsilon_0}+i\left[(\epsilon_r+1)-\frac{\sigma_I q}{\omega_0\epsilon_0}\right]}\frac{q}{\omega_0^2}e^{-2qz_0}\right)\\
&= -\frac{\omega}{\pi}\frac{c^2}{(2\pi)^2}\mathrm{Im}\left(\int d\mathbf{q}\frac{-\frac{q\sigma_R}{\omega_0\epsilon_0\sigma_I}+i\left[\frac{(\epsilon_r-1)}{\sigma_I}-\frac{q}{\omega_0\epsilon_0}\right]}{-\frac{q\sigma_R}{\omega_0\epsilon_0\sigma_I}+i\left[\frac{(\epsilon_r+1)}{\sigma_I}-\frac{q}{\omega_0\epsilon_0}\right]}\frac{q}{\omega_0^2}e^{-2qz_0}\right).
\end{aligned}\tag{A1}$$

Now we take the imaginary part and write

$$\begin{aligned}
\rho &= -\frac{\omega}{\pi}\frac{c^2}{(2\pi)^2}\left(\int d\mathbf{q}\frac{-\frac{q\sigma_R}{\omega_0\epsilon_0\sigma_I}\left[-\frac{(\epsilon_r+1)}{\sigma_I}+\frac{q}{\omega_0\epsilon_0}+\frac{(\epsilon_r-1)}{\sigma_I}-\frac{q}{\omega_0\epsilon_0}\right]}{\left(\frac{q\sigma_R}{\omega_0\epsilon_0\sigma_I}\right)^2+\left[\frac{(\epsilon_r+1)}{\sigma_I}-\frac{q}{\omega_0\epsilon_0}\right]^2}\frac{q}{\omega_0^2}e^{-2qz_0}\right)\\
&= \frac{\omega}{\pi}\frac{c^2}{(2\pi)^2}\left(\int d\mathbf{q}\left[\frac{\frac{2q\sigma_R}{\omega_0\epsilon_0\sigma_I}\frac{1}{\sigma_I}}{\left(\frac{q\sigma_R}{\omega_0\epsilon_0\sigma_I}\right)^2+\left[\frac{(\epsilon_r+1)}{\sigma_I}-\frac{q}{\omega_0\epsilon_0}\right]^2}\right]\frac{q}{\omega_0^2}e^{-2qz_0}\right)
\end{aligned}$$

At the no loss limit $\frac{\sigma_R}{\sigma_I}\to 0$ we get

$$\rho = \frac{\omega}{\pi}\frac{c^2}{(2\pi)^2}\left(\int d\mathbf{q}\frac{\frac{2q\sigma_R}{\omega_0\epsilon_0\sigma_I}\frac{1}{\sigma_I}}{\left[\frac{(\epsilon_r+1)}{\sigma_I}-\frac{q}{\omega_0\epsilon_0}\right]^2}\frac{q}{\omega_0^2}e^{-2qz_0}\right).$$

Substituting $q = q_0 u = [(\epsilon_r+1)\,\omega_0\epsilon_0/\sigma_I]u$, where q_0 is a resonant k vector we write

$$\begin{aligned}
\rho &= \frac{\omega}{\pi}\frac{c^2}{(2\pi)^2}\left(\int dqd\theta q^2\frac{\frac{2q_0u}{\omega_0\epsilon_0\sigma_I}\frac{\sigma_R}{\sigma_I}}{\left(\frac{(\epsilon_r+1)}{\sigma_I}\right)^2(1-u)^2}\frac{1}{\omega_0^2}e^{-2uq_0z_0}\right)\\
&= \frac{\omega}{\pi}\frac{c^2}{(2\pi)^2}\left(\int dqd\theta q^2\frac{\frac{2\frac{(\epsilon_r+1)\omega_0\epsilon_0}{\sigma_I}u}{\omega_0\epsilon_0\sigma_I}\frac{\sigma_R}{\sigma_I}}{\left(\frac{(\epsilon_r+1)}{\sigma_I}\right)^2(1-u)^2}\frac{1}{\omega_0^2}e^{-2uq_0z_0}\right)\\
&= \frac{\omega}{\pi}\frac{c^2}{(2\pi)^2}\left(\int dqd\theta q^2\frac{\frac{2u}{\sigma_I}\frac{\sigma_R}{\sigma_I}}{\left(\frac{(\epsilon_r+1)}{\sigma_I}\right)(1-u)^2}\frac{1}{\omega_0^2}e^{-2uq_0z_0}\right)\\
&= \frac{\omega c^2}{(2\pi)^2}\left(\int dqd\theta q^2\frac{\frac{2}{\sigma_I}}{\frac{(\epsilon_r+1)}{\sigma_I}}\left(\frac{1}{\pi}\frac{\frac{\sigma_R}{\sigma_I}u}{(1-u)^2}\right)\frac{1}{\omega_0^2}e^{-2uq_0z_0}\right)\\
&= \frac{\omega c^2}{(2\pi)^2}\left(\int dud\theta u^2q_0^3\frac{\frac{2}{\sigma_I}}{\frac{(\epsilon_r+1)}{\sigma_I}}\left(\frac{1}{\pi}\frac{\frac{\sigma_R}{\sigma_I}u}{(1-u)^2}\right)\frac{1}{\omega_0^2}e^{-2uq_0z_0}\right).
\end{aligned}$$

We express the resonant wave vector q_0, which is excited, in terms of the far-field wave vector k

$$q_0 = k\eta,$$

where η is the confinement factor and obtain

$$\begin{aligned}\rho &= \frac{\omega c^2}{(2\pi)^2}\left(\int dud\theta u^2 k^3\eta^3 \frac{\frac{2}{\sigma_I}}{\frac{(\epsilon_r+1)}{\sigma_I}}\left(\frac{1}{\pi}\frac{\frac{\sigma_R}{\sigma_I}u}{(1-u)^2}\right)\right.\\ &\left.\times\frac{1}{\omega_0^2}e^{-2uq_0z_0}\right)\\ &= \frac{\omega c^2}{(2\pi)^2}\left(k^3\eta^3\frac{2}{(\epsilon_r+1)}\frac{1}{\omega_0^2}e^{-2k\eta z_0}\right)\\ &= \frac{\omega}{(2\pi^2)}\left(k\eta^3\frac{1}{(\epsilon_r+1)}e^{-2k\eta z_0}\right).\end{aligned}$$

In conclusion, the scaling of the density of states is

$$\rho \propto \eta^3 e^{-2k\eta z_0},$$

similarly to the scaling of the spontaneous emission due to electronic transitions with the QED treatment in Ref. [18].

[1] Daniel C. Harris and Michael D. Bertolucci, *Symmetry and Spectroscopy: An Introduction to Vibrational and Electronic Spectroscopy* (Dover publications, New York, 1989).

[2] David M. Bishop, Molecular vibrational and rotational motion in static and dynamic electric fields, Rev. Mod. Phys. **62**, 343 (1990).

[3] Ekaterina I. Galanzha, Robert Weingold, Dmitry A. Nedosekin, Mustafa Sarimollaoglu, Jacqueline Nolan, Walter Harrington, Alexander S. Kuchyanov, Roman G. Parkhomenko, Fumiya Watanabe, Zeid Nima, *et al.*, Spaser as a biological probe, Nat. Commun. **8**, 1 (2017).

[4] Chanaka Rupasinghe, Weiren Zhu, and Malin Premaratne, in *2014 IEEE Photonics Conference* (IEEE, San Diego, CA, USA, 2014), p. 16, https://ieeexplore.ieee.org/abstract/document/6994967.

[5] Avi Schroeder, Daniel A. Heller, Monte M. Winslow, James E. Dahlman, George W. Pratt, Robert Langer, Tyler Jacks, and Daniel G. Anderson, Treating metastatic cancer with nanotechnology, Nat. Rev. Cancer **12**, 39 (2012).

[6] Daniel Rodrigo, Odeta Limaj, Davide Janner, Dordaneh Etezadi, F. Javier, García de Abajo, Valerio Pruneri, and Hatice Altug, Mid-infrared plasmonic biosensing with graphene, Science **349**, 165 (2015).

[7] M. Y.u Tretyakov, E. A. Serov, M. A. Koshelev, V. V. Parshin, and A. F. Krupnov, Water dimer rotationally resolved millimeter-wave spectrum observation at room temperature, Phys. Rev. Lett. **110**, 093001 (2013).

[8] David DeMille, Quantum computation with trapped polar molecules, Phys. Rev. Lett. **88**, 067901 (2012).

[9] Ira N. Levine, *et al.*, *Molecular Spectroscopy* (Wiley, New York, 1975).

[10] M. Oldani, M. Andrist, A. Bauder, and A. G. Robiette, Pure rotational spectra of methane and methane-d4 in the vibrational ground state observed by microwave Fourier transform spectroscopy, J. Mol. Spectrosc. **110**, 93 (1985).

[11] Yiqiao Tang and Adam E. Cohen, Optical chirality and its interaction with matter, Phys. Rev. Lett. **104**, 163901 (2010).

[12] Yiqiao Tang and Adam E. Cohen, Enhanced enantioselectivity in excitation of chiral molecules by superchiral light, Science **332**, 333 (2011).

[13] Raphael Lescanne, Samuel Deleglise, Emanuele Albertinale, Ulysse Reglade, Thibault Capelle, Edouard Ivanov, Thibaut Jacqmin, Zaki Leghtas, and Emmanuel Flurin, Irreversible qubit-photon coupling for the detection of itinerant microwave photons, Phys. Rev. X **10**, 021038 (2020).

[14] E. U. Condon, The absolute intensity of the nebular lines, Astrophys. J. **79**, 217 (1934).

[15] V. V. Klimov and V. S. Letokhov, Quadrupole radiation of an atom in the vicinity of a dielectric microsphere, Phys. Rev. A **54**, 4408 (1996).

[16] Prashant K. Jain, Debraj Ghosh, Roi Baer, Eran Rabani, and A. Paul Alivisatos, Near-field manipulation of spectroscopic selection rules on the nanoscale, Proc. Natl. Acad. Sci. **109**, 8016 (2012).

[17] A. M. Kern and Olivier J. F. Martin, Strong enhancement of forbidden atomic transitions using plasmonic nanostructures, Phys. Rev. A **85**, 022501 (2012).

[18] Nicholas Rivera, Ido Kaminer, Bo Zhen, John D. Joannopoulos, and Marin Soljačić, Shrinking light to allow forbidden transitions on the atomic scale, Science **353**, 263 (2016).

[19] G. Karl and J. D. Poll, On the quadrupole moment of the hydrogen molecule, J. Chem. Phys. **46**, 2944 (1967).

[20] A. Goldman, J. Reid, and L. S. Rothman, Identification of electric quadrupole O_2 and N_2 lines in the infrared atmospheric absorption spectrum due to the vibration-rotation fundamentals, Geophys. Res. Lett. **8**, 77 (1981).

[21] Matthias Germann, Xin Tong, and Stefan Willitsch, Observation of electric-dipole-forbidden infrared transitions in cold molecular ions, Nat. Phys. **10**, 820 (2014).

[22] Alessandro Ciattoni, Claudio Conti, and Andrea Marini, Multipolar terahertz absorption spectroscopy ignited by graphene plasmons, Commun. Phys. **2**, 111 (2019).

[23] D. N. Basov, M. M. Fogler, and F. J. García de Abajo, Polaritons in van der Waals materials, Science **354**, aag1992 (2016).

[24] Marinko Jablan, Hrvoje Buljan, and Marin Soljačić, Plasmonics in graphene at infrared frequencies, Phys. Rev. B **80**, 245435 (2009).

[25] Alexander N. Grigorenko, Marco Polini, and K. S. Novoselov, Graphene plasmonics, Nat. Photonics **6**, 749 (2012).

[26] F. Javier Garcia de Abajo, Graphene plasmonics: Challenges and opportunities, ACS Photonics **1**, 135 (2014).

[27] Itai Epstein, David Alcaraz, Zhiqin Huang, Varun-Varma Pusapati, Jean-Paul Hugonin, Avinash Kumar, Xander M. Deputy, Tymofiy Khodkov, Tatiana G. Rappoport, Jin-Yong Hong, *et al.*, Far-field excitation of single graphene plasmon cavities with ultracompressed mode volumes, Science **368**, 1219 (2020).

[28] Iris Crassee, M. Orlita, M. Potemski, Andrew L. Walter, M. Ostler, Th. Seyller, I. Gaponenko, Jianing Chen, and A. B. Kuzmenko, Intrinsic terahertz plasmons and magnetoplasmons in large scale monolayer graphene, Nano Lett. **12**, 2470 (2012).

[29] David Alcaraz Iranzo, Sebastien Nanot, Eduardo J. C. Dias, Itai Epstein, Cheng Peng, Dmitri K. Efetov, Mark B. Lundeberg, Romain Parret, Johann Osmond, Jin-Yong Hong, *et al.*, Probing the ultimate plasmon confinement limits with a van der Waals heterostructure, Science **360**, 291 (2018).

[30] Michele Tamagnone, Antonio Ambrosio, Kundan Chaudhary, Luis A. Jauregui, Philip Kim, William L. Wilson, and Federico Capasso, Ultra-confined mid-infrared resonant phonon polaritons in van der Waals nanostructures, Sci. Adv. **4**, 7189 (2018).

[31] Iban Amenabar, Simon Poly, Wiwat Nuansing, Elmar H. Hubrich, Alexander A. Govyadinov, Florian Huth, Roman Krutokhvostov, Lianbing Zhang, Mato Knez, Joachim Heberle, *et al.*, Structural analysis and mapping of individual protein complexes by infrared nanospectroscopy, Nat. Commun. **4**, 2890 (2013).

[32] Long Ju, Baisong Geng, Jason Horng, Caglar Girit, Michael Martin, Zhao Hao, Hans A. Bechtel, Xiaogan Liang, Alex Zettl, Y. Ron Shen, *et al.*, Graphene plasmonics for tunable terahertz metamaterials, Nat. Nanotechnol. **6**, 630 (2011).

[33] Philippe Tassin, Thomas Koschny, and Costas M. Soukoulis, Graphene for terahertz applications, Science **341**, 620 (2013).

[34] Claude Cohen-Tannoudji, Bernard Diu, and Frank Laloe, *Quantum Mechanics*, edited by Claude Cohen-Tannoudji, Bernard Diu, Frank Laloe (Wiley-VCH, 1986), Vol. 2, p. 626. ISBN 0-471-16435-6.

[35] D. B. Lawson and J. F. Harrison, Distance dependence and spatial distribution of the molecular quadrupole moments of H_2, N_2, O_2, and F_2, J. Phys. Chem. A **101**, 4781 (1997).

[36] D. Reuter, D. E. Jennings, and J. W. Brault, The $v = 1 \rightarrow 0$ quadrupole spectrum of N_2, J. Mol. Spectrosc. **115**, 294 (1986).

[37] F. Wijnands, J. B. Pendry, F. J. Garcia-Vidal, P. M. Bell, P. J. Roberts, and L. Marti'n Moreno, Green's functions for Maxwell's equations: Application to spontaneous emission, Opt. Quantum Electron. **29**, 199 (1997).

[38] E. Purcell, Spontaneous emission probabilities at radio frequencies, Phys. Rev. **69**, 00 (1946).

[39] Stephen Sanders, Asher May, Alessandro Alabastri, and Alejandro Manjavacas, Extraordinary enhancement of quadrupolar transitions using nanostructured graphen, ACS Photonics **5**, 3282 (2018).

[40] Asaf Farhi and David J. Bergman, Analysis of a Veselago lens in the quasistatic regime, Phys. Rev. A **90**, 013806 (2014).

[41] Sandra Eibenberger, John Doyle, and David Patterson, Enantiomer-specific state transfer of chiral molecules, Phys. Rev. Lett. **118**, 123002 (2017).

[42] Sharly Fleischer, Yan Zhou, and Robert W. Field, Keith A. Nelson, Molecular orientation and alignment by intense single-cycle THz pulses, Phys. Rev. Lett. **107**, 163603 (2011).

[43] H. Harde, Soren Keiding, and D. Grischkowsky, THz commensurate echoes: Periodic rephasing of molecular transitions in free-induction decay, Phys. Rev. Lett. **66**, 1834 (1991).

[44] Oleg Mitrofanov, Leonardo Viti, Enrico Dardanis, Maria Caterina Giordano, Daniele Ercolani, Antonio Politano, Lucia Sorba, and Miriam S. Vitiello, Near-field terahertz probes with room-temperature nanodetectors for subwavelength resolution imaging, Sci. Rep. **7**, 44240 (2017).

[45] Lev Davidovich Landau, J. S. Bell, M. J. Kearsley, L. P. Pitaevskii, E. M. Lifshitz, and J. B. Sykes, *Electrodynamics of Continuous Media* (Elsevier, 2013), Vol. 8.

[46] Roi Baer and Eran Rabani, Theory of resonance energy transfer involving nanocrystals: The role of high multipoles, J. Chem. Phys. **128**, 184710 (2008).

[47] Ho Trung Dung, Ludwig Knöll, and Dirk-Gunnar Welsch, Intermolecular energy transfer in the presence of dispersing and absorbing media, Phys. Rev. A **65**, 043813 (2002).

[48] Asaf Farhi and Aristide Dogariu, Purcell factors and Förster-resonance energy transfer in proximity to helical structures, Phys. Rev. A **106**, 1013708 (2022).

[49] Eleftherios N. Economou, *Green's Functions in Quantum Physics* (Springer, Berlin Heidelberg, 1983), Vol. 3.